Comparison of prenatal ultrasonography and fetal MRI in diagnosing neural tube defects: A prospective observational study

Mengchun Sun[1], Gan Gao[1], Benzhang Tao[1], Hui Wang[1], and AIJIA SHANG[1]

[1]Chinese PLA General Hospital

August 16, 2022

Abstract

Objective: To compare the diagnostic accordance rate between prenatal ultrasonography and fetal magnetic resonance imaging (MRI) for varied neural tube defects (NTDs), and introduce detailed prenatal imaging characteristics of multiple NTDs. Design: A prospective observational study Setting: Chinese PLA General Hospital Population: The fetuses developing possible NTDs. Method: We prospectively followed up the fetuses and collected their data of prenatal ultrasonography, fetal MRI, and postnatal MRI examinations. Fisher's exact test was used to perform the statistical analysis. A P value of < 0.05 was considered statistically significant. Main Outcome Measures: The diagnostic accordance rate of prenatal ultrasonography and fetal MRI for each involved NTD, prenatal imaging characteristics of each involved NTD. Results: We included 119 fetuses with 11 NTDs. Ultrasonography revealed a significant advantage in diagnosing spina bifida ($P < 0.05$) and a relative advantage in diagnosing intraspinal cyst, dermal sinus, and skin mass. MRI demonstrated intraspinal lipoma better ($P < 0.05$), and was appropriate for identifying complex malformations. Both could accurately diagnose tethered cord syndrome (without intraspinal lesions), meningocele/myelomeningocele, and sacrococcygeal teratoma. Conclusions: Prenatal ultrasonography and fetal MRI have different advantages in diagnosing NTDs. To ensure a prompt and accurate diagnosis, it is crucial for clinicians to raise awareness of the prenatal imaging characteristics of various NTDs, which will lay a solid foundation for better fetal prognosis. Funding: This study was supported by the Capital's Funds for Health Improvement and Research (CFH2022-2-5022). Keywords: prenatal ultrasonography, fetal magnetic resonance imaging, neural tube defects, pregnancy, diagnosis, fetus

Introduction

Neural tube defects (NTDs) develop during the gestational period and cause various abnormalities of the central nervous system. Early detection, diagnosis, and treatment of NTDs can improve clinical outcomes. Noninvasive prenatal imaging examinations, including ultrasonography and magnetic resonance imaging (MRI),[1]are vital for monitoring fetuses and identifying congenital abnormalities. Previous studies have reported some typical imaging features of NTDs and compared the advantages of prenatal ultrasonography and fetal MRI from various aspects.[2-8] However, detailed descriptions of prenatal imaging manifestations of each type of NTDs are still lacking.

Moreover, no study has applied postnatal MRI examination results as a diagnostic criterion to compare the diagnostic ability of prenatal ultrasonography and fetal MRI for diverse NTDs.

In this study, we aimed to compare the diagnostic accordance rate of prenatal ultrasonography and fetal MRI for various NTDs and recommend more specific and individualized prenatal examination methods for each type of NTDs to increase the positive outcome rates. Furthermore, we aimed to introduce detailed prenatal imaging characteristics of multiple NTDs using both ultrasonography and MRI. To the best of our knowledge, this is the first prospective comparative study on prenatal imaging that includes most cases and types of NTDs and summarizes the most comprehensive prenatal imaging characteristics of various NTDs.

Methods

We prospectively followed up fetuses who possibly developed NTDs and were admitted to the Department of Neurosurgery, Chinese PLA General Hospital between July 2020 and October 2021. We advised pregnant women to undergo ultrasound examination at the Department of Ultrasonic Diagnosis and fetal MRI examination at the Department of Medical Imaging in the same gestational week. According to the results of the examinations, a multidisciplinary consultation was held by neurosurgeons, obstetricians, pediatric surgeons, sonographers, and radiologists to analyze fetal disease conditions and evaluate fetal prognosis. Referring to the clinicians' objective assessments, the pregnant women and their families made independent decisions on further pregnancy processes. If the pregnant woman decided to carry the baby to term, her baby underwent another MRI examination within 1 month postnatally at the Department of Medical Imaging to confirm the prenatal diagnosis. We collected prenatal and postnatal clinical and imaging data from these fetuses.

Mindray Resona 8T ultrasound machines (Mindray Bio-Medical Electronics Co., CHN) with 1–6-MHz curved array probes were used to perform transabdominal 2D and 3D-ultrasound examinations on the pregnant women. All scans were independently performed by a chief physician with more than 10 years of experience.

Fetal MRI was performed with a 3.0-T magnet (Spectra, Siemens Medical Solution, USA) equipped with a phased-array body coil. Half-Fourier acquisition single-shot turbo spin-echo (HASTE) and true fast imaging with steady procession (true FISP) sequences (TR/TE, 1400/130; thickness, 3 mm; field, 280 × 280 mm – 360 × 360 mm) were used to acquire T2-weighted images in the sagittal, coronal, and axial planes. For each sequence. The imaging process for each sequence was approximately 20 s for the region of interest and approximately 40 s for the whole body. To eliminate subjective bias and personal preferences, a professional imaging technician manipulated the equipment, and an experienced radiologist read and interpreted the images and wrote the reports without knowing the results of previous ultrasound examinations.

We administered oral chloral hydrate at a recommended dose of 50–100 mg/kg (up to a maximum of 2 g) as a sedative to the infants 30 min before the 3.0-T MRI examination (Spectra, Siemens Medical Solution, USA).[9] We acquired T1-weighted, T2-weighted, and fat-depressed images in the sagittal, coronal, and axial planes (TR/TE, 1400/130; thickness, 3–5 mm; field, 280 × 280 mm–360 × 360 mm). Scanning and analysis were performed by a skilled technician and chief radiologist, respectively.

SPSS software (version 26.0, IBM Corp., USA) was used to analyze the data. Using the manifestations of postnatal MRI examinations as the diagnostic criteria, we performed Fisher's exact test to compare the diagnostic accordance rate between prenatal ultrasonography and fetal MRI for each disease. A P value $<$ 0.05 was considered statistically significant.

Results

Overall, 119 fetuses were included in this study. The distribution of diseases and the comparison of diagnostic accordance rates between prenatal ultrasonography and fetal MRI examinations are shown in**Table 1** . The following 11 NTDs were included: spina bifida, tethered cord syndrome (TCS) (without intraspinal lesions), intraspinal lipoma, intraspinal cyst, meningocele/myelomeningocele, dermal sinus, skin mass, sacrococcygeal teratoma, syringomyelia, sacrococcygeal hypoplasia, and caudal regression syndrome. We found that prenatal ultrasonography revealed a significant advantage in diagnosing spina bifida than that revealed by fetal MRI ($P < 0.05$); fetal MRI, demonstrated intraspinal lipoma better than that demonstrated by prenatal ultrasonography ($P < 0.05$); there was no statistically significant difference between the two techniques in observing intraspinal cyst, dermal sinus and skin mass ($P > 0.05$); and both prenatal ultrasonography and fetal MRI could accurately diagnose TCS (without intraspinal lesions), meningocele/myelomeningocele, and sacrococcygeal teratoma. Due to sample size limitations, Fisher's exact test could not compare the differences in syringomyelia, sacrococcygeal hypoplasia, and caudal regression syndrome between the two techniques. We investigated the imaging characteristics of these 11 NTDs using prenatal ultrasonography and fetal MRI as follows:

Spina bifida

Prenatal ultrasonography showed normal vertebrae with parallel "beads-on-string" double bands in the

midsagittal plane, and the fusion of bilateral vertebral arches could be observed at the sacral segment in the coronal plane.[10] Spina bifida showed unclear ossification centers of the vertebral arches, unclosed high-echo bony structures, or disordered vertebrae at the lumbosacral segment (**Fig. 1A**). In fetal MR images, the true FISP sequence could clearly demonstrate the vertebrae with a low signal, which are in significant contrast to surrounding soft tissues. In the region of spina bifida, especially at the sacrum, we found disconnected vertebral arches, although this sign might be obscure (**Fig. 1B**).

Tethered cord syndrome (without intraspinal lesions)

Excluding intraspinal lesions, TCS results from a thickened (diameter [?] 2 mm) and tight filum terminale.[11-13] By both ultrasonography and MRI, we observed an elongated low-lying conus medullaris without a cone shape appearance (**Fig. 2A**). Especially in the sagittal images of fetal MRI, the spinal cord was stretched and moved backward (**Fig. 2B**). The thickened filum terminale was fatty and showed a linear high-echo signal in ultrasound (**Fig. 2C**).

Intraspinal lipoma

Intraspinal lipoma presents as a high-echo mass on ultrasonography (**Fig. 3A**) but shows a low signal on the HASTE/T2 sequence of fetal MRI. We found thickened, blunt, and malformed conus medullaris mingled with a low-signal lipoma on the axial MR images (**Fig. 3B**). On the sagittal MRI image, the spinal cord tethered by a lipoma moved backward and remained fixed (**Fig. 3C**). Due to the lipoma, the conus medullaris had lost its normal appearance and could not be located at an exact vertebra level, especially when the lipoma was a mixed type (no specific interface between the lipoma and cord).

Intraspinal cyst

On ultrasound images, an intraspinal cyst presented as an anechoic oval area with a definite boundary at the termination of the conus medullaris, and the conus medullaris maintained a regular cone-like appearance despite the cyst (**Fig. 4A**). On MR images, an intraspinal cyst was identified based on the sign of a cystic oval area with a high signal as that of the cerebrospinal fluid (CSF) in the HASTE/T2 sequence (**Fig. 4B**). Some indirect signs, such as a widened lumbar or sacral spinal canal, in the sagittal and coronal planes also indicated a possible intraspinal cyst (**Fig. 4C** and**D**).

Meningocele/Myelomeningocele

Meningocele or myelomeningocele was easily identified using prenatal ultrasonography and fetal MRI. On ultrasound images, meningocele manifested as a lumbosacral anechoic cystic mass protruding from the spinal canal, with or without skin covering (**Fig. 5A**), while myelomeningocele contained additional high-echo strips, i.e., the spinal cord and cauda equina, in the bulge (**Fig. 5B**). In the axial and sagittal MR images of the meningocele, it was conspicuous that the cystic mass communicated with the subarachnoid space and contained CSF, which was covered by thin skin or membrane (**Fig. 5C** and**D**). The sagittal MR image of the myelomeningocele showed that the spinal cord and cauda equina had also herniated into the cystic mass (**Fig. 5E**), forming the "Ω sign" (**Fig. 5F**). Both meningocele and myelomeningocele are accompanied by disconnected lumbosacral vertebral arches, indicating spina bifida aperta.

Dermal sinus

Dermal sinus was observed as a "finger-like" subcutaneous anechoic crack,[14] i.e., a sinus tract extending to the dura sac on the ultrasound images (**Fig. 6A**), which was accompanied by a skin tag or discontinuous echo signal from defective skin in that area. The tract presented as a diagonal lumbosacral subcutaneous low-signal on the sagittal MR images (**Fig. 6B**).

Skin mass

A skin mass indicated a subcutaneous and intraspinal communicating lipoma, instead of a simple cutaneous lesion. Ultrasonography revealed a lumbosacral skin mass with a high-echo signal, while the echo signal of the fetal dorsal skin remained intact (**Fig. 7A**). The skin mass was identified as a lesion with a slightly

low signal on the HASTE/T2 sequence of the fetal MRI, and the dorsal skin outline appeared uneven (**Fig. 7B**).

Sacrococcygeal teratoma

Sacrococcygeal teratoma is the most common tumor in fetuses and neonates.[15] According to the classification of Altman et al., sacrococcygeal teratoma can be divided into four subtypes based on location: Type I is predominantly external and contains a few presacral components; Type II exists externally but significantly extends into the pelvis; Type III predominantly lies in the pelvis with an obvious external mass; and Type IV has a complete presacral tumor without an external part.[16] In the cases included in this study, two fetuses had teratoma. In Case 1, the external teratoma presented as a huge sacrococcygeal cystic mass with internal heterogeneous signals, while a minimal component extended to the presacral space, which was classified as Type II (**Fig. 8A** and**B**). In Case 2, the tumor existed mostly in the pelvis and abdomen, showing mixed cystic and solid signals, that is, a Type III teratoma (**Fig. 8C**). Notably, the Case 2 was also diagnosed with congenital anal atresia and perineal vestibular fistula at birth.

Syringomyelia

It was difficult to detect the fetal syrinx cavity using ultrasonography because of a sketchy image appearance and low resolution (**Fig. 9A**). Compared with prenatal ultrasonography, fetal MRI provided more information. Among the three planes of MR images, the axial plane produced the best image for the syrinx cavity, in which a CSF space in the central canal was identified (**Fig. 9B, C,** and **D**). Syringomyelia is more possible to be observed in fetuses with NTDs that caused strong traction on the spinal cord, such as Chiari malformation, intraspinal lipoma, and meningocele/myelomeningocele.

Sacrococcygeal hypoplasia

Sacrococcygeal hypoplasia presented as an undeveloped sacrum and coccyx with dysplastic sacral nerves. Ultrasound images showed obscure or no bony-echo signals from the sacrum and coccyx. Instead, a high-echo sacrococcygeal intraspinal mass was observed, indicating an intraspinal lipoma. This can result in an extremely low-lying conus medullaris, causing difficulty in identifying the conus medullaris (**Fig. 10A** and **B**). On sagittal MR images, we observed an undeveloped sacrum and a sacrococcygeal intraspinal lipoma with low signal intensity (HASTE/T2 sequence) filling the space of the incomplete vertebrae (**Fig. 10C, D,** and **E**).

Caudal regression syndrome

Ultrasonography showed that the conus medullaris in fetuses with caudal regression syndrome was bluntly terminated and located at a level that was higher than normal (**Fig. 11A**). Fetal MRI can perfectly present the typical imaging characteristics of caudal regression syndrome. Particularly on sagittal and coronal MR images, the fetuses with caudal regression syndrome had a “blunt-ending” and “club-shaped” conus medullaris that terminated abruptly at a higher vertebra level (**Fig. 11B** and **C**), with the caudal nerve roots arranged in anterior and posterior bundles, known as double-bundle arrangement of the caudal nerves (**Fig. 11D**).[7]The sacrum was dysplastic or absent (**Fig. 11D**).

Discussion

Main Findings

In this study, we described the imaging features of fetal NTDs and compared the diagnostic accordance rates between prenatal ultrasonography and fetal MRI.

Strengths and Limitations

This study covered the imaging characteristics of involved NTDs at both fetal and infancy stage, presenting a complete imaging diagnostic process. Meanwhile, we took the results of postnatal MRI examination as the gold standard to confirm the prenatal diagnoses, which promised the accuracy and reliability of the statistical

results. To the best of our knowledge, this is a prospective prenatal imaging study that investigates most types of fetal NTDs and introduces comprehensive ultrasound imaging and MRI characteristics.

This study has some limitations. The data were obtained from a single medical center. Due to the follow-up duration and possible termination of pregnancy, withdrawal is unavoidable. Moreover, the positive rate of prenatal deficits is related to clinicians' professional skills. Therefore, we hope to conduct a well-designed multicenter prospective study with a larger sample size in the future.

Interpretation

In our study, ultrasonography showed a significantly higher diagnostic accordance rate for spina bifida, which could be attributed to its sensitivity to bones with strong high-echo signals. Although the true FISP sequence of fetal MRI could well image the spine,[17] the vertebrae with low signals seem indistinct among surrounding tissues. Interestingly, we encountered two cases of bony malformations during the study enrolment process. The abnormal vertebrae were clear on the ultrasound images, particularly the 3D-ultrasound images, but unclear on the MR images (**Fig. 12**). Because of induced labor, these two cases were excluded from our study; therefore, their prenatal diagnosis could not be verified after birth. However, our data still shows that ultrasonography could better identify bony abnormalities than MRI.

Our results revealed the advantages of fetal MRI in identifying intraspinal lipomas. The authors agreed that MRI can effectively image soft tissues and physical details.[18] In the HASTE sequence of fetal MRI, intraspinal lipoma shows low signal intensities, strongly contrasting with the high signals of CSF and the equal signals of the spinal cord. Conversely, because ultrasonography shows different soft tissues with similar high-echo signals, small lipomas may be ignored. Therefore, MRI is a more suitable diagnostic method for fetal intraspinal lipoma than ultrasonography.

We found no statistical difference in the diagnostic accordance rate between ultrasonography and MRI for intraspinal cysts, dermal sinuses, and skin masses. We observed an edge contrast between both examinations, indicating that ultrasonography may be better than MRI in identifying these NTDs. For intraspinal cysts, ultrasonography identified 89.5% of the cases, whereas MRI identified approximately 73.7%. We concluded on two causes of a missed diagnosis by MRI: (1) the same high signal in T2-weighted MR images might interfere with intraspinal cyst and CSF and (2) the cyst wall might be too thin to develop. MRI can omit a few-millimeter-wide subcutaneous sinus tract of the dermal sinus, particularly when the image layers are thick. A small lumbosacral skin mass that is compressed by the uterine wall may also be difficult to capture by MRI. Therefore, a limited sample size may explain the statistical results. We believe that a further study involving more cases would support our views.

We found that ultrasonography and MRI showed comparable abilities in diagnosing TCS without intraspinal lesions, meningocele/myelomeningocele, and sacrococcygeal teratoma as their typical imaging features make them easily identifiable. A low-lying conus medullaris indicates TCS. Our previous studies have confirmed that both ultrasonography and MRI can be used to identify the fetal conus medullaris.[19,20] Meningocele and myelomeningocele belong to open dysraphic abnormalities, which is a prominent characteristic distinguishable from other diseases. Sacrococcygeal teratomas show conspicuous cystic or solid masses outside the spinal canal or inside the pelvis and abdomen. MRI provide more information on fetal sacrococcygeal teratoma[21], but regarding the identification of lesions, we consider that ultrasonography also provides accurate information.

In our study, two of the four syringomyelia cases were diagnosed using MRI, but none was identified by ultrasonography. The diagnostic accordance rates of both ultrasonography and MRI were unsatisfactory. The fetal intramedullary syrinx cavity is tiny and difficult to image; a subtle syrinx cavity could be confused with a physically dilated central canal in fetuses. Notably, none of the four syringomyelia cases was associated with Chiari malformation. Because Chiari malformation predominantly causes syringomyelia,[22] radiologists may consider the possibility of syringomyelia once they identify typical signs of fetal Chiari malformation ("lemon sign" and "banana sign").[23] Therefore, a single fetal syringomyelia can easily be overlooked, which could account for the low positive rate in our study. We suggest that MRI should be the first-choice

examination for fetal syringomyelia, owing to its high imaging resolution. Sacrococcygeal hypoplasia and caudal regression syndrome occurs with multiple deficits such as bony malformations, dysplastic nerves, and intraspinal lipomas. In our study, all cases with these two diseases were diagnosed using MRI alone. We attributed this result to the distinguishable imaging signals of the different structures in MR images. Therefore, we recommend to use fetal MRI to identify complicated combined abnormalities.

Based on previous studies and clinical experience, we believe that meningoceles should be distinguished from sacrococcygeal teratomas because of their similar cystic signals on ultrasonography and MRI. We summarize the differential points as follows: (1) cystic sacrococcygeal teratoma is located at a position lower than that of meningocele and can extend into the presacral space;[24] (2) meningocele has a symmetric cystic mass, but cystic teratoma has an asymmetric one;[24] (3) cystic teratoma compared to meningocele may be larger and have a thinner wall; (3) meningocele communicates with the subarachnoid space and coexists with TCS, but teratoma can exist alone; and (4) the meningocele is completely cystic and can contain a few caudal equina, but the teratoma can contain both cystic and solid components.

Conclusion

Prenatal ultrasonography and fetal MRI have different advantages in diagnosing congenital deficits: ultrasonography is more suitable for spina bifida, while MRI is more suitable for intraspinal lipoma. Ultrasonography provides more valuable information on fetal bony malformations, cystic lesions, and cutaneous abnormalities, while MRI is more appropriate for diagnosing subtle intraspinal lesions and complex abnormalities. Both ultrasonography and MRI accurately identify obvious malformations. To ensure a prompt and accurate diagnosis, it is crucial for clinicians to raise awareness of the prenatal imaging characteristics of various NTDs, which will lay a solid foundation for better fetal prognosis.

Acknowledgements: None

Disclosures of Interest: The authors have stated that they had no interests which might be perceived as posing a conflict or bias.

Contribution to Authorship

Conception: Mengchun Sun, Aijia Shang

Planning: Mengchun Sun, Gan Gao, Aijia Shang

Carrying out: Mengchun Sun, Gan Gao, Benzhang Tao, Hui Wang

Analyzing: Mengchun Sun, Gan Gao, Benzhang Tao, Aijia Shang

Writing up: Mengchun Sun

Details of Ethics Approval: This study was approved by the institutional review board of PLA General Hospital (No. S2022-189-01, date of approval: 2019. 04. 25) and followed the tenets of the Declaration of Helsinki. Each pregnant woman and her husband provided written informed consent for the research and publication of the results.

Funding : This study was supported by the Capital's Funds for Health Improvement and Research (CFH2022-2-5022).

References

1. Morel B, Friszer S, Jouannic JM, Ducou Le Pointe H, Blondiaux E, Garel C. Prenatal sacral anomalies leading to the detection of associated spinal cord malformations. Fetal Diagn Ther. 2017;42:294-301.
2. Duczkowska A, Bekiesinska-Figatowska M, Herman-Sucharska I, Duczkowski M, Romaniuk-Doroszewska A, Jurkiewicz E, et al. Magnetic resonance imaging in the evaluation of the fetal spinal canal contents. Brain Dev. 2011;33:10-20.
3. Pierre-Kahn A, Sonigo P. Lumbosacral lipomas: in utero diagnosis and prognosis. Childs Nerv Syst. 2003;19:551-4.

4. Sakr S, Mohan Y, Malik A, Malik G, Gonik B. Prenatal diagnosis of congenital dermal sinus. AJP Rep. 2015;5:e43-5.
5. van Heurn LJ, Coumans ABC, Derikx JPM, Bekker MN, Bilardo KM, Duin LK, et al. Factors associated with poor outcome in fetuses prenatally diagnosed with sacrococcygeal teratoma. Prenat Diagn. 2021;41:1430-8.
6. Thorne A, Pierre-Kahn A, Sonigo P. Antenatal diagnosis of spinal lipomas. *Childs* Nerv Syst. 2001;17:697-703.
7. Kumar Y, Gupta N, Hooda K, Sharma P, Sharma S, Kochar P, et al. Caudal regression syndrome: a case series of a rare congenital anomaly. Pol J Radiol. 2017;82:188-92.
8. Wang J, Zhou Q, Fu Z, Xiao X, Lu Y, Zhang G, et al. MRI evaluation of fetal tethered-cord syndrome: correlation with ultrasound findings and clinical follow-up after birth. Clin Radiol. 2021;76:314.e1-8.
9. National Institute for Health and Care Excellence: Sedation in under 19s: using sedation for diagnostic and therapeutic procedures (Clinical guideline CG112). https://www.nice.org.uk/guidance/cg112 [26 August 2021].
10. D'Addario V, Rossi AC, Pinto V, Pintucci A, Di Cagno L. Comparison of six sonographic signs in the prenatal diagnosis of spina bifida. J Perinat Med. 2008;36:330-4.
11. Salbacak A, Büyükmumcu M, Malas MA, Karabulut AK, Seker M. An investigation of the conus medullaris and filum terminale variations in human fetuses. Surg Radiol Anat. 2000;22:89-92.
12. Pinto FC, Fontes RB, Leonhardt Mde C, Amodio DT, Porro FF, Machado J. Anatomic study of the filum terminale and its correlations with the tethered cord syndrome. Neurosurgery. 2002;51:725-30.
13. Tubbs RS, Oakes WJ. Can the conus medullaris in normal position be tethered? Neurol Res. 2004;26:727-31.
14. Sakr S, Mohan Y, Malik A, Malik G, Gonik B. Prenatal diagnosis of congenital dermal sinus. AJP Rep. 2015;5:e43-5.
15. Brace V, Grant SR, Brackley KJ, Kilby MD, Whittle MJ. Prenatal diagnosis and outcome in sacrococcygeal teratoma: a review of cases between 1992 and 1998. Prenat Diagn. 2000;20:51–5.
16. Altman RP, Randolph JG, Lilly JR. Sacrococcygeal teratoma: American Academy of Pediatrics Surgical Section Survey-1973. J Pediatr Surg. 1974;9:389–98.
17. Walter WR, Alizai H, Bruno M, Portugal S, Burke CJ. Real-time dynamic 3-T MRI assessment of spine kinematics: a feasibility study utilizing three different fast pulse sequences. Acta Radiol. 2021;62:58–66.
18. Shekdar K, Feygin T. Fetal neuroimaging. Neuroimaging Clin N Am. 2011;21:677–703, ix.
19. Sun M, Tao B, Gao G, Wang H, Shang A. Conus medullaris migration during the third trimester: a retrospective study. Prenat Diagn. 2021;41:1643–8.
20. Sun M, Tao B, Gao G, Wang H, Shang A. Determination of the normal conus medullaris level in term infants: the role of MRI in early infancy. J Neurosurg Pediatr. 2022;29:100–5.
21. Danzer E, Hubbard AM, Hedrick HL, Johnson MP, Wilson RD, Howell LJ, et al. Diagnosis and characterization of fetal sacrococcygeal teratoma with prenatal MRI. AJR Am J Roentgenol. 2006;187:W350–6.
22. Saletti V, Farinotti M, Peretta P, Massimi L, Ciaramitaro P, Motta S, et al. The management of Chiari malformation type 1 and syringomyelia in children: a review of the literature. Neurol Sci. 2021;42:4965–95.
23. Kunpalin Y, Richter J, Mufti N, Bosteels J, Ourselin S, De Coppi P, et al. Cranial findings detected by second-trimester ultrasound in fetuses with myelomeningocele: a systematic review. BJOG. 2021;128:366–74.
24. McGahan JP, Pilu G, Nyberg DA. Neural tube defects and the spine. In*Diagnostic Imaging of Fetal Anomalies* , Nyberg DA, McGahan JP, Pretorius DH, Pilu G (eds). Lippincott Williams & Wilkins: Philadelphia, 2003;291–334.

Figure legends

Fig. 1: Spina bifida A: Prenatal ultrasound image showing bilateral disconnected vertebral arches (white

arrows). B: Sagittal MR image showing no bony abnormalities of the fetal spine.

Fig. 2: Tethered cord syndrome (without intraspinal lesions) A: Ultrasound image showing an elongated low-lying conus medullaris at S1 vertebra level (white arrow). B: Sagittal MR image showing an abnormal fetal conus medullaris moving backward (white arrow). C: Prenatal ultrasound image showing a thickened fatty filum terminale with a high-echo signal (white arrow).

Fig. 3: Intraspinal lipoma A: Prenatal ultrasound image showing a lumbosacral intraspinal high-echo mass (arrow). B: Axial MR image showing abnormal fetal conus medullaris mixed with low-signal fat (white arrow). C: Sagittal MR image showing fetal conus medullaris tethered by lipoma and moving backward (white arrow).

Fig. 4: Intraspinal cyst. A: Prenatal ultrasound image showing a lumbar intraspinal oval anechoic area (white arrow). B: Axial fetal MR image showing an intraspinal cystic lesion with a clear boundary and high signal similar to that of the cerebrospinal fluid (white arrow). C, D: Sagittal (C) and coronal (D) fetal MR images showing a widened lumbosacral spinal canal (white arrow).

Fig. 5 : Meningocele/myelomeningocele. A: Prenatal ultrasound image showing a lumbosacral protruding anechoic cystic mass (white arrow). B: Prenatal ultrasound image showing high-echo strips in the cystic mass (white arrow). C, D: Axial (C) and sagittal (D) MR images showing cystic mass communicating with the subarachnoid space and containing CSF (black arrows). E: Axial MR image showing spinal cord and cauda equina herniating into the cystic mass (white arrow). F: Herniated spinal cord forming a "Ω sign" in sagittal MR image (black arrow).

Fig. 6: Dermal sinus. A: Prenatal ultrasound image showing a "finger-like" subcutaneous anechoic crack (white arrow). B: Sagittal MR image showing a diagonal lumbosacral subcutaneous low-signal (white arrow).

Fig. 7 : Skin mass. A: Prenatal ultrasound image showing a lumbosacral skin mass with high-echo signal (white arrow). B: HASTE/T2 sequence of fetal MR image showing a lesion with a slightly low signal and an uneven dorsal skin outline (white arrow).

Fig. 8 : Sacrococcygeal teratoma. **Case1** : A, B: Prenatal ultrasound image (A) and fetal MR image (B) showing a huge sacrococcygeal cystic mass with internal heterogeneous signals inside and a minimal component extending to the presacral space (white arrows), that is, Type II. **Case2** : C: Fetal MR image showing a heterogeneous tumor existing mostly in the pelvic and abdomen (white arrow) with an obvious external mass (red arrow), that is, Type III.

Fig. 9 : Syringomyelia. A: No fetal syrinx cavity observed on the prenatal ultrasound image. B: Axial fetal MR image showing a cerebrospinal fluid space in the central canal (white arrow). C, D: Sagittal (C) and axial (D) postnatal MR images verifying a syrinx cavity (white arrows).

Fig. 10 : Sacrococcygeal hypoplasia. A, B: Sagittal (A) and coronal (B) prenatal ultrasound images showing a high-echo sacrococcygeal intraspinal mass instead of normal bony-echo signals in the sacrum and coccyx. C: HASTE/T2 sequence of fetal MRI showing undeveloped sacrum and a sacrococcygeal intraspinal lipoma with low signal filling the space of incomplete vertebrae formation (white arrow). D: T2-weighted sequence postnatal MR image verifying undeveloped sacrum below the S2 vertebra (white arrow). E: Fat-depressed sequence of postnatal MR image showing a low-signal intraspinal lipoma pulling the spinal cord (white arrow).

Fig. 11 : Caudal regression syndrome. A: Prenatal ultrasound image showing a blunt termination of the spinal cord at a vertebra level that is higher than the normal (white arrow). B, C: Sagittal (B) and coronal (C) MR images showing a "blunt-ending" and "club-shaped" conus medullaris abruptly terminating at a higher vertebra level. D: Postnatal MR image showing dysplastic sacrum and the caudal nerve roots arranged in anterior and posterior bundles, known as, double-bundle arrangement of the caudal nerves.

Fig. 12 : Bony malformation. **Case 1** : A: Prenatal ultrasound image showing an abnormal paravertebral bony structure with a high-echo signal (white arrow). B: 3D-ultrasound image showing the rebuilding of the

fetal spine and showing an abnormal osteophyte on the right of the L3–4 vertebrae, implying a malformed vertebral arch (white arrow). C: Fetal MR image showing no obvious bony malformations.**Case 2:** D: Prenatal ultrasound image showing disordered arrangement of the fetal vertebrae (white arrow). E: 3D-ultrasound image showing the rebuilding of the fetal spine and showing multiple malformed vertebrae (white arrow). F: Fetal MRI showing partial abnormal vertebrae (white arrow).

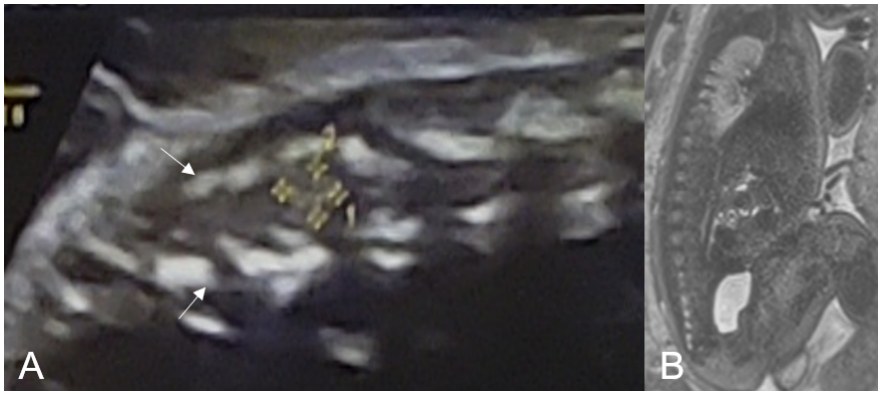

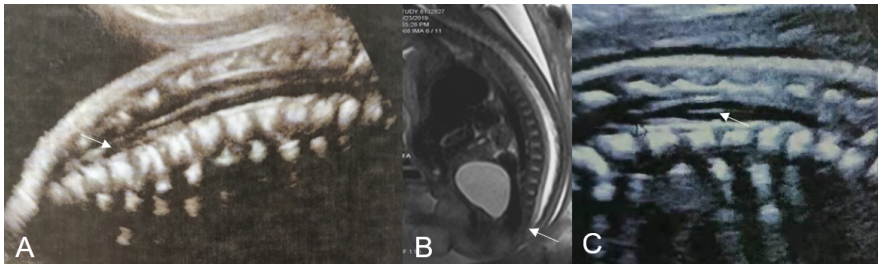

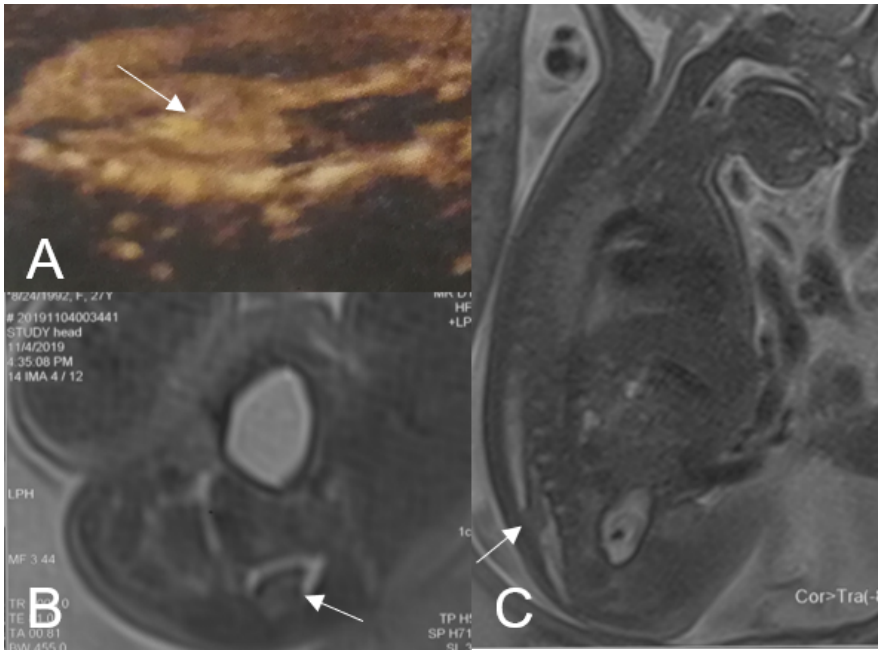

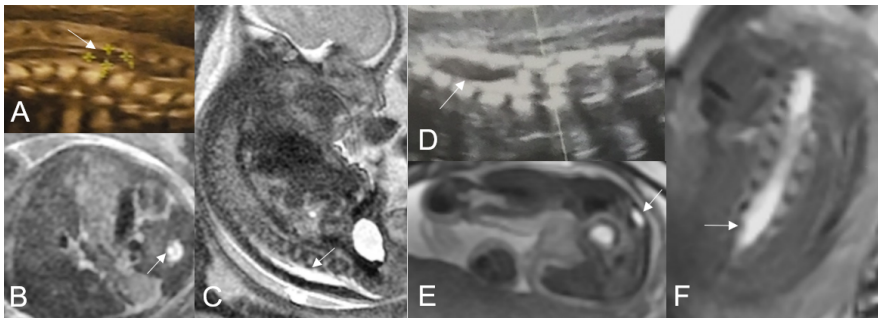

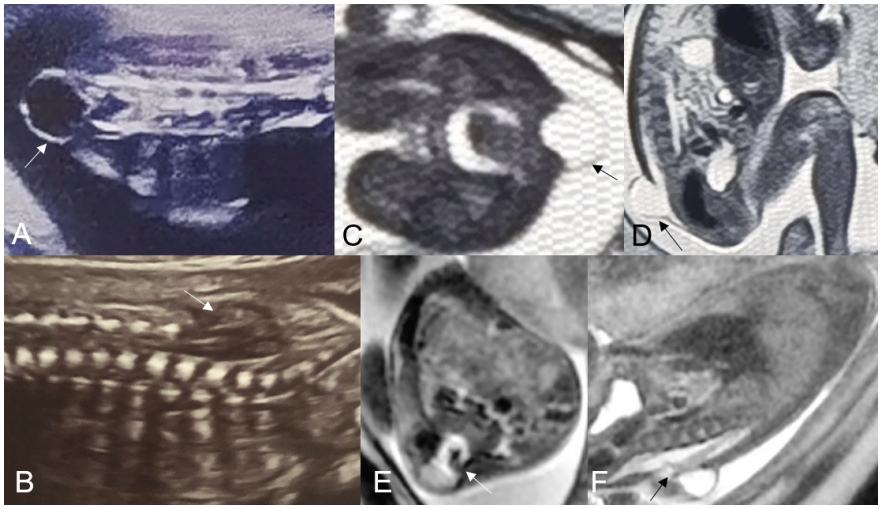

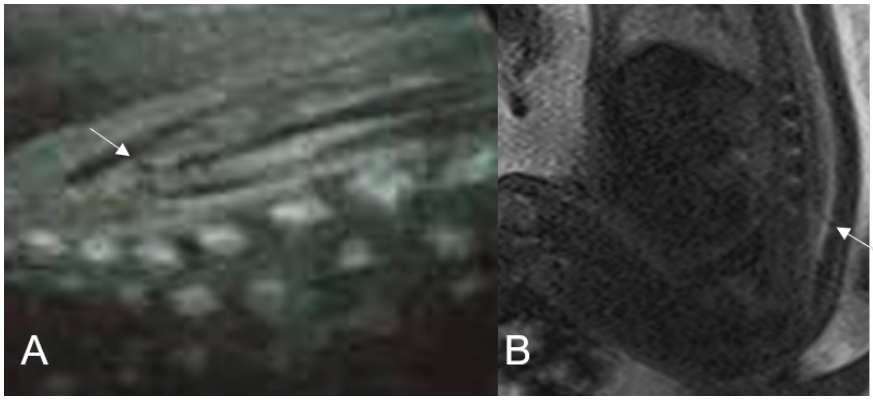

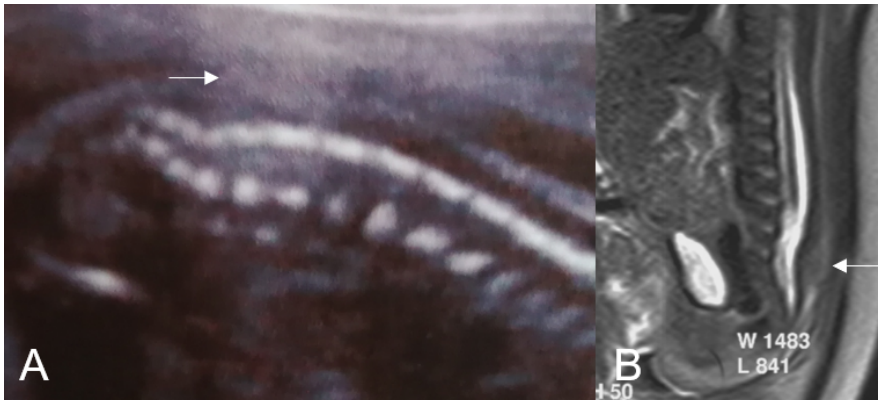

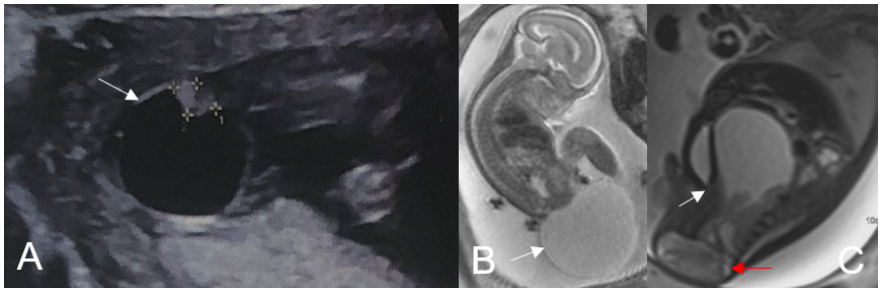

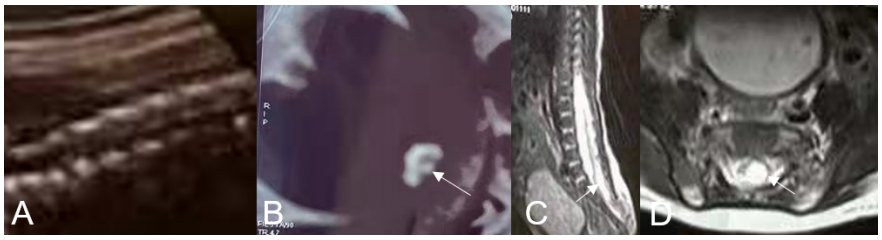

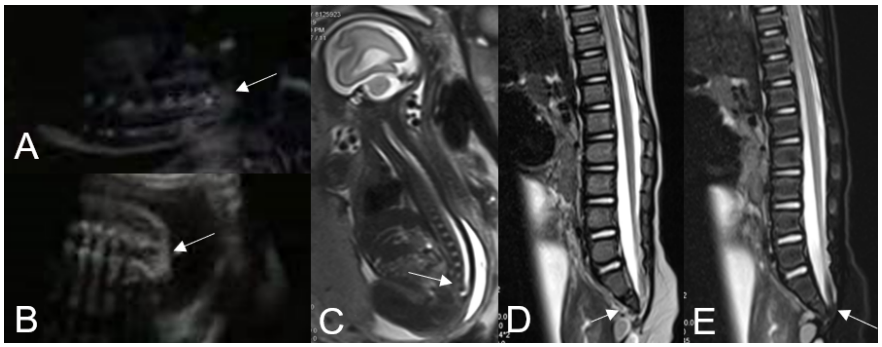

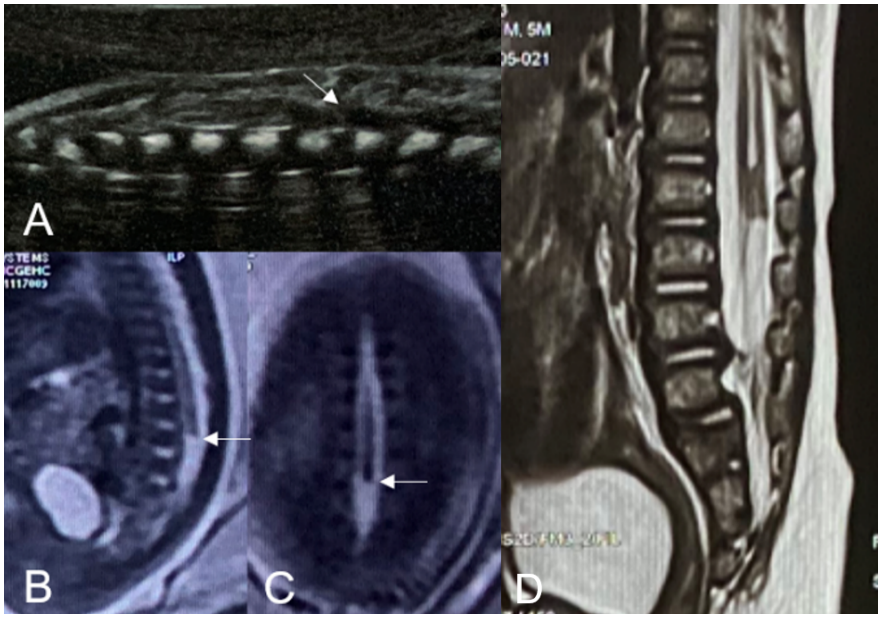

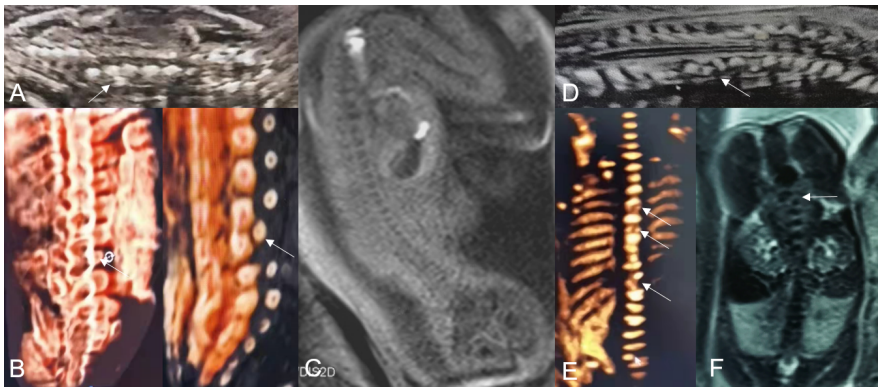

Hosted file

table.docx available at https://authorea.com/users/501418/articles/581902-comparison-of-prenatal-ultrasonography-and-fetal-mri-in-diagnosing-neural-tube-defects-a-prospective-observational-study